IV INTENSITIES AND CROSS SECTIONS OF Ne, H_2, N_2, NO AND O_2 CLUSTERS IN A MOLECULAR BEAM.

IV.1 INTRODUCTION

Persuing our earlier effort (ref. 1), we have investigated molecular beams of Ne, H_2, N_2, NO, and O_2 clusters. The temperature and pressure dependence of the ion signals have been measured for masses up to three times the monomer mass.

The neutral beam is attenuated by argon- or helium-gas in a scatterbox. While the total collision cross section itself is of interest, it serves at the same time to check what neutral parent belongs to a certain ion mass (ref. 1). Only for monomers and dimers we were able to determine a "clean" cross section.

For Ar we have been able to plot the intensities vs. reduced source pressures P_{red}, such that for all source temperatures T_0, a single curve is obtained for each ion mass. The aim of this investigation is to test whether a similar reduction is also possible for another noble gas, Ne, for a nearly noble gas, H_2, and also for diatomic molecules, N_2 and NO.

For H_2 and the paramagnetic gases NO and O_2, the magnetic properties of the dimer have been compared with those of the monomers, using a Rabi type deflection magnet of 40 cm length and a maximum field gradient of 20 kGauss cm^{-1}.

In addition to the insertion of this deflection magnet, the original set-up described in ref. 1 has been changed by replacing the small mass spectrometer magnet by a more powerful one (a switching magnet, model 1038, Spectromagnetic Industries, 14 cm pole diameter). At 900 eV ion energy the mass range extends up to 2500 amu.

All measurements have been done using a 26 μ nozzle diameter. The distance between source and scatterbox amounts to 65 cm, that between the source and detector slit to 195 cm. Good collimation of the beam is ensured by the rectangular opening of the scatterbox, 0.4x12 mm^2, and the slit in front of the detector, 0.8 x 8 mm^2. Extra collimation at the source was tried but never felt necessary. A view of the apparatus is given in fig. IV.1.

IV.2. THE INTENSITIES

In fig. IV.2a the intensities are drawn as a function of the reduced pressure for the isotopes of the Ne-monomer and for their dimers. The Ne-gas used has the natural composition, 90.92% ^{20}Ne, 8.82% ^{22}Ne, 0,257% ^{21}Ne. The figure shows the ^{20}Ne monomer intensity divided by a factor 10; in consequence it coincides with the ^{22}Ne monomer; the omitted signal of the other isotope scales according to its natural abundance.

the scatterbox Sb and the Rabi type magnet R. The beam is collimated by a slit of the scatterbox and the detector slit D. Then the cluster beam enters the ionizer I; the ions are mass selected in magnet MSM and amplified by electron multiplier M. Reversing the magnetic field in MSM the ions can be used for further experiments ("ion scattering"). All distances given are in mm.

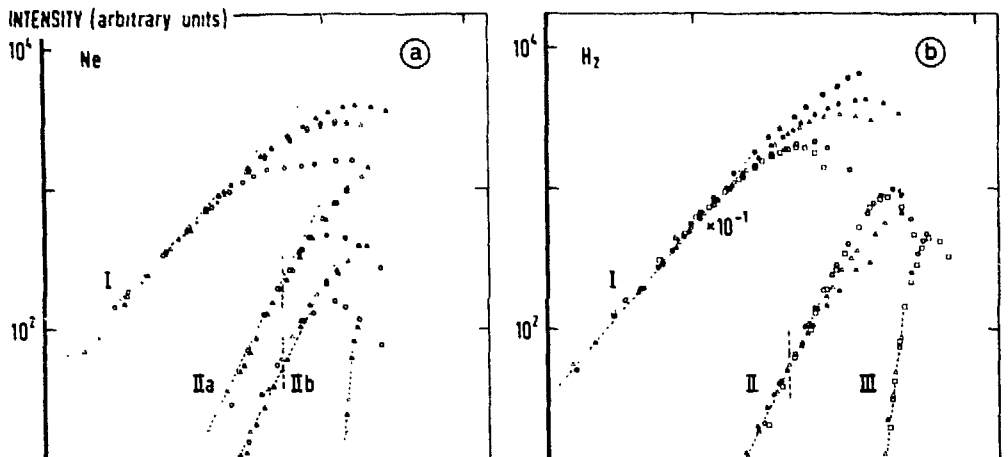

Fig. IV.2. Intensity vs. reduced pressure for Ne (a) and H_2 *(b)*. In the left part of the figure the symbol I corresponds to the $^{20}Ne^+$ intensity divided by a factor 10; the $^{22}Ne^+$ intensity at T_0= 65K is indicated by x. The symbol IIa corresponds to $^{20}Ne_2^+$, IIb to $^{20}Ne^{22}Ne^+$, and III to $^{20}Ne_3^+$. In the right part of the figure the symbol I belongs to H_2^+, II to H_3^+ and III to H_5^+. The monomer intensity (I) is displayed divided by a factor 10. The intensities are measured at temperatures T_0 = 100K (▲), T_0 = 65 K (Δ ,x), and T_0 = 33 K (O). For H_2 we have added the intensities for T_0 = 273K (●, monomer only) and T_0 = 28 K (□).
The abscissa represents the true pressure P_0 in torr for T_0 = 65 K.
At other temperatures reduction factors P_0/P_{red} are applied for each ion mass, see table IV.I. At the reduced pressure $\tilde{P}_L$ the dimer signal becomes contaminated by fragments of larger clusters.

For a source temperature T_0=65K the reduced pressure P_{red} equals the true source pressure P_0; for other temperatures the reduction factors are given in table IV.1.

No scaling other than for the monomer ion isotopes is applied in vertical direction. At higher pressures the intensity curves start to diverge, the high temperature ones always above the low temperature ones. This behaviour stems from the fact that at lower source temperatures the production of heavier clusters takes place at lower reduced pressures, causing a decrease of intensity. Also, heavier clusters start to appear; Ne_5^+ ions are observed but not shown in fig. IV.2.

The dimer ion isotopes have a constant ratio of intensities, $I_{40}/I_{42} \simeq 4$, as expected from statistical considerations.

In fig. IV.2b the results for H_2 are given. As discussed in ref. 2 we have observed ions H_2^+, H_3^+ and H_5^+; also higher masses were detected (ref. 2), but

are not considered in the present work. For the reduction factors P_0/P_{red} see table IV.1.

For the monomer ion signals the diverging tendency at high pressures is similar to that observed for Ne and Ar (ref. 1). However, for the H_3^+– ion the sequence is reversed. In our interpretation the reversal is caused by significant fragmentation of heavy clusters into H_3^+-ions in the ionizer.

In fig. IV.3a and 3b the intensities are given for N_2 and NO, respectively, for temperatures T_0 between 130 K and 300 K. In table IV.1 the reduction factors P_0/P_{red} are given. Signals of heavier clusters have been observed, for instance up to N_{14}^+, but are not displayed in fig. IV.3. Contrary to the case of H_2, here the ions of even mass have intensities stronger than those of odd mass. For instance, fourty times the N_3^+-signal is observed on N_4^+, whereas fifty times the H_6^+-signals equals roughly the H_5^+–signal (ref. 2).

The pressure range where we can draw a straight line through the results in fig. IV.2 and 3 is called the onset region. The cross section results of the following section show that in this region the monomer (dimer) ion signals originate from neutral monomers (dimers).

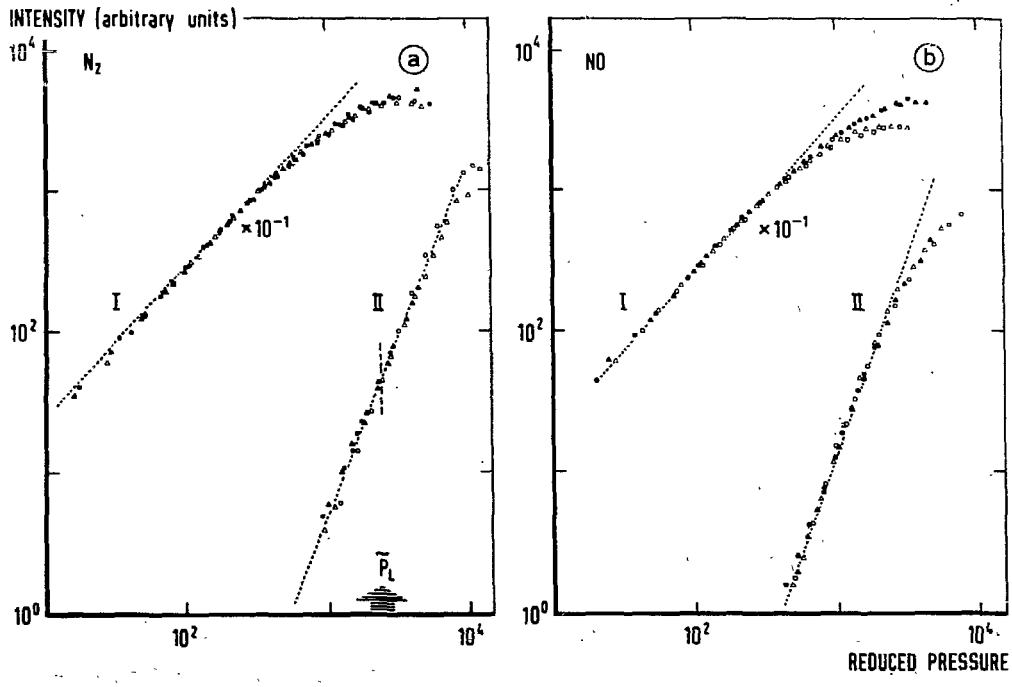

caption to fig IV.3

Fig. IV.3. Intensities vs. reduced pressure for N_2 (a) and NO (b).
The intensities are measured at source temperatures T_0 = 296 K (●), T_0 = 223 K (▲), T_0 = 173 K (Δ), and T_0 = 133 K (O). The abscissa represents the true pressure P_0 in torr for T_0 = 233 K. At other temperatures reduction factors P_0/P_{red} have been applied, see table IV.1. The monomer ion signal (I) is displayed, divided by a factor 10; The dimer ion signals N_4^+ and $(NO)_2^+$ are indicated by II. For N_2 the reduced value $\tilde{P}_L$ is indicated; no P_L can be defined for NO.

TABLE IV.1

	m	28	33	65	100	296	(K)
Ne^+	1	—	.48 ± .03	1	1.7 ± .1	—	
Ne_2^+	2	—	.24 ± .02	1	2.0 ± .1	—	
H_2^+	1	.44 ± .02	.52 ± .03	1	1.30 ± .05	3.5 ± .2	
H_3^+	2	.16 ± .01	.23 ± .01	1	2.1 ± .1	—	
H_5^+	3	.11	.16	1	—	—	

	m	133	173	223	296	(K)
N_2^+	1	.65 ± .05	.88 ± .05	1	1.4 ± .1	
N_4^+	2	.25 ± .02	.53 ± .05	1	2.5 ± .2	
NO^+	1	.63 ± .03	.90 ± .05	1	1.32 ± .1	
$(NO)_2^+$	2	.31 ± .02	.55 ± .05	1	2.4 ± .1	

Table IV.1. Reduction factors $f = P_0/P_{red}$, $I^+_{m,0} \sim P_0^{\alpha_m} / T_0^{\alpha_m \beta_m}$

TABLE IV.2

gas	α_1	β_1	α_2	β_2	α_3	β_3
Ne	1.1 ± .1	1.1 ± .1	2.0 ± .1	1.9 ± .1	—	—
H_2	1.1 ± .1	.9 ± .1	2.0 ± .1	2.0 ± .1	7.8 ± .5	2.7 ± .1
N_2	1.1 ± .1	.9 ± .1	2.5 ± .2	2.85 ± .1	—	—
NO	1.1 ± .1	.9 ± .1	2.8 ± .1	2.5 ± .1	—	—

Table IV.2. Exponents α_m *and* β_m for the intensities in the onset region.

In the onset region the measured intensities $I^+_{m,0}$ are approximately proportional to $P_0^{\alpha_m} / T_0^{\alpha_m \cdot \beta_m}$, m = 1 for the Ne^+, H_2^+, N_2^+ and NO^+ signals, m = 2 for the Ne_2^+, H_3^+, N_4^+ and $(NO)_2^+$ signals. Values for α_m and β_m are shown in table IV.2.

The pressure dependence of $I^+_{m,0}$ is in accordance with expectation, $\alpha_1 \simeq 1$. For $I^+_{2,0}$ one expects a proportionality with the squared density of the monomer in the source.

Experimentally we find $\alpha_2 = 2.0 \pm 0.1$ for Ne, Ar (ref.1) and H_2; for N_2, NO and O_2, however, we find $\alpha_2 = 2.5 \pm .2$, $2.8 \pm .1$ and $2.7 \pm .2$, respectively.

Even a simple equilibrium theory for dimer concentration predicts a much more complicated temperature dependence than the proportionality with $T_0^{-\alpha_2 \cdot \beta_2}$. However, for the limited temperature range investigated this approximation gives the right reduction factor P_0/P_{red} within 7% for Ne and H_2, within 6% for N_2 and within 9% for NO.

With respect to ref. 1 the scattering technique has been improved attaching an ionization gauge directly to the 80 K scatterbox (see also ref.3). The filament of the gauge is mounted under tension to prevent geometrical changes during operation. Thereby, the reproducibility is kept within 1% per day. During long measuring periods the gauge is not swiched off for weeks. To attenuate the neutral beam a pressure of about 10^{-4} torr is maintained in the scatterbox; for the unattenuated beam the box is pumped down to about $2.\times10^{-7}$ torr.

In fig. IV.4a and 4b the total collision cross section results for Ne and H_2 are displayed with a light and a heavy scattering partner, respectively. As in ref.1 we are able to define a pressure limit $\bar{P}_L$, below which the dimer ion signal corresponds to a neutral dimer parent. The range for $\bar{P}_L$ indicated in fig. IV.2, 3, 4 and 5 is obtained by dividing the P_L values by the reduction factors for the dimer intensities (see table IV.1) A general criterion will be discussed in the next section.

The velocity of the beam molecules, v_1, has been calculated from the source temperature T_0 assuming full isentropic expansion, $v_1 = (2C_p\,T_0)^{\frac{1}{2}}$; C_p is the specific heat at constant pressure per unit mass. The average relative

Fig. IV.4. Apparent cross section vs. reduced pressure for Ne (a) and H_2 (b) of monomers (I) and dimers (II).
The different symbols correspond to different temperatures, T_0 = 100 K (▲), T_0 = 65 K (Δ); for Ne the results at T_0 = 33 K (O), for H_2 those at T_0 = 166 K (●) and T_0 = 30 K (O) are added. As target molecule He is used for Ne, and Ar for H_2. The ordinates are logarithmic; at all values of T_0 the avarage value of σ_1 is taken equal to unity for both Ne and H_2. The abscissa represents the true pressure P_0 for T_0 = 65 K; at other temperatures reduction factors have been applied, see table IV.1. For T_0 = 166 K interpolated reduction factors are used. For $P_{red} \leq \bar{P}_L$ the dimer cross section is determined. The results for both Ne isotopes are shown together. The dimer measurements for Ne do not extend to very low pressures because of detector noise due to residual background ions. For Ne no variation in σ_2/σ_1 is found, for H_2 a slight variation with T_0 is apparent. The shaded regions for $\bar{P}_L$ are obtained by a reduction of P_L with the same factors as for the dimer intensities, see table IV.1.

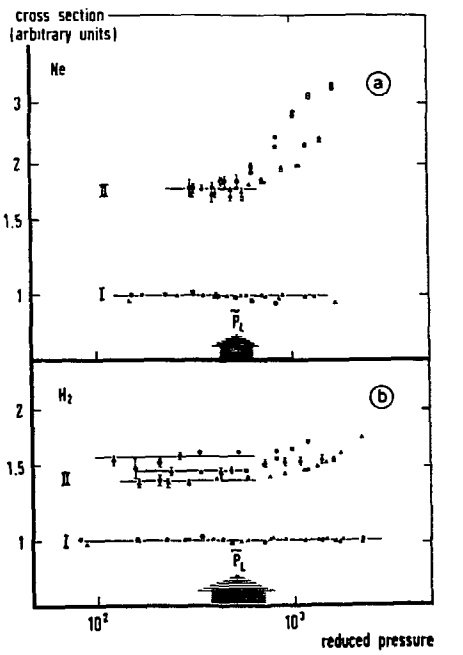

velocity v for different scattering partners has been calculated from v_1 and the thermal velocity of the scatter gas, α_s ; $v = (v_1^2 + \alpha_s^2)^{\frac{1}{2}}$. Fig. IV.4 shows that the velocity dependence of σ_2/σ_1, the ratio of dimer and monomer cross section, is small or negligible. For this reason we refrained from a more accurate velocity determination.

In fig. IV.5a and b similar results are given for N_2 and NO. No velocity dependence of σ_2/σ_1 is detected. With a heavy scattering partner, the value of σ_2/σ_1 equals 1.34 ± .02 for NO, 1.43 ± .03 for N_2, and 1.40 ± .02 for O_2. The ratio found for Ar (cf. ref. 1) is $\sigma_2/\sigma_1 = 1.39 \pm .02$, for Ne $\sigma_2/\sigma_1 = 1.35 \pm .05$. For H_2 the values range from $\sigma_2/\sigma_1 = 1.36 \pm .02$, at $v_1 \simeq 1200$ msec^{-1}, to $\sigma_2/\sigma_1 = 1.55 \pm .04$, at $v_1 \simeq 1900$msec^{-1}.

For the light scattering partner (He) larger σ_2/σ_1 ratios are found, generally: $\sigma_2/\sigma_1 = 1.64 \pm .02$ for N_2, $\sigma_2/\sigma_1 = 1.57 \pm .05$ for O_2; $\sigma_2/\sigma_1 = 1.77 \pm .02$ for Ne and $\sigma_2/\sigma_1 = 1.96 \pm .06$ for H_2. For the molecular system NO the ratio σ_2/σ_1 is found slightly smaller, $\sigma_2/\sigma_1 = 1.51 \pm .02$.

The angular resolution correction is applied to σ_2/σ_1 following ref. 4. For the heavy scattering partner, where the interaction is dominated by a r^{-6}–attraction, this correction equals roughly the experimental uncertainty. The relative correction due to the spread in relative velocity is the same for σ_2 and σ_1 (ref. 5.). The light collision partner poses the problem that the angular resolution correction according to ref. 4 becomes rather inaccurate for two reasons. Firstly, the velocity dependence is not in agreement with a pure r^{-6}–potential. Secondly, the velocity of the target molecules is comparable to v_1; in this case the formulas of ref. 4 are not properly valid. Lack of a better procedure has forced us neverthe-

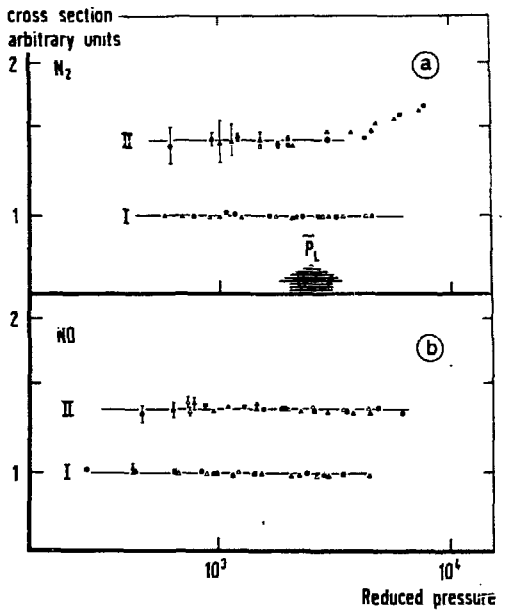

Fig. IV.5. Apparent cross section vs. reduced velocity for N_2 (a) and NO (b) of monomers (I) and dimers (II).
The different symbols correspond to different temperatures, $T_0 = 296$ K (●), $T_0 = 223$ K (▲), $T_0 = 173$ K (Δ), and $T_0 = 133$ K (O). The abscissa represents the true pressure P_0 in torr for $T_0 = 233$ K; for other temperatures a reduction is applied equal to that for the intensities (table IV.1). For both N_2 and NO, Ar is used as target gas. For all temperatures σ_1 is independent of the source pressure and is taken equal to unity. For N_2 a pressure $\tilde{P}_L$ is defined; from reduced pressures $P_{red} \leq \tilde{P}_L$ the dimer cross section σ_2 is determined. For NO the cross section σ_2 is constant up to the highest pressures, where ion signals of larger clusters are already present. Both for N_2 and NO, the ratio σ_2/σ_1 is equal for all T_0.

less, to use the correction method of ref. 4. The statistical error given for σ_2/σ_1 does not include the uncertainty of this correction

The discussion of the ratio σ_2/σ_1 for a heavy scattering partner can be based on the expression for the total collision cross section (ref. 6)

$$\sigma_{tot} = 8.083(C_6/\hbar v)^{2/5} \qquad \text{(IV.1)}$$

From eq. IV.1 follows $C_{6.d}/C_{6.m} = (\sigma_2/\sigma_1)^{2/5}$. Consequently, $\sigma_2/\sigma_1 = 1.32$ yields $C_{6.d} = 2C_{6.m}$ (ref. 1). Observed ratios 1.34 - 1.45 correspond to $C_{6.d}/C_{6.m}$ between 2.0 and 2.5 This ratio appears reasonable to us; theoretical predictions for $C_{6.d}/C_{6.m}$ do not exist at this moment.

For H_2-Ar scattering and wherever He is used as scattering partner, glories in the total collision cross section might have been expected. However, due to the velocity averaging for He (average velocity in the 80K scatterbox 600 $msec^{-1}$) the glories are smoothed out entirely. With the H_2– beam this averaging effect is much smaller because here the heavy and slow partner is in the scatterbox. Here, σ_2/σ_1 is found to vary slightly over the large velocity range, v_1 between 800 and 1850 $msec^{-1}$.

If one neglects all possible inelastical events (rotational excitation and dissociation of the loosely bound $(H_2)_2$-complex), one can calculate σ_2/σ_1 under simplifying assumptions concerning the interaction potential. In fig. IV.6 results of such a calculation are shown.

The monomer cross section is calculated (ref.7) for the Lennard Jones potential with ε and R_m taken from ref. 3. Our measured monomer cross section σ_1 (fitted to the calculated value at 1180 m sec^{-1}) agrees with the calculations to within the experimental error. The spread in relative velocity due to the thermal velocity of the target gas is indicated by the horizontal bars on σ_1.

In fig. IV.6. the experimental points of σ_2 are derived from the calculated σ_1 and the measured ratios σ_2/σ_1.
We calculated (ref. 7) a dimer cross section for various sets of Lennard Jones parameters. A reasonable fit is shown in fig. IV.6, for $C_{6.d} = 2.5C_{6.m}$ (IIa) and $2.7C_{6.m}$ (IIb); the product εR_m is kept constant and taken equal to the monomer value because this guarantees the absence of glory undulation in σ_2/σ_1.
The $C_{6.d}/C_{6.m}$ value obtained are similar to the results for the heavier systems.

IV.4 THE MAXIMUM PRESSURE P_L FOR PURE DIMER BEAMS

One main result of this work is the firm establishment of experimental conditions under which the dimer ion signal corresponds to pure dimers, with negligible contamination from fragments of heavier clusters. For each source

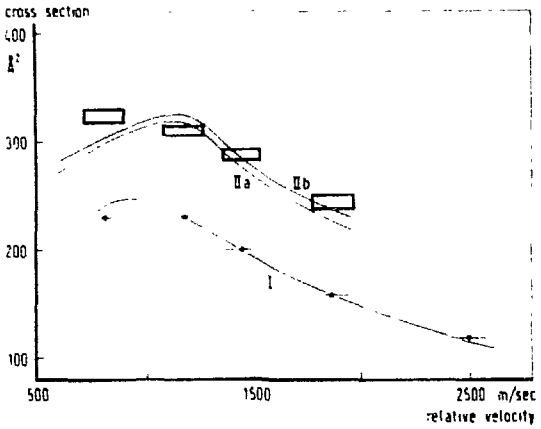

Fig. IV.6. Calculated and measured cross section σ_2 and σ_1 vs. velocity for H_2-Ar.
The curve indicated by (I) represents the calculated monomer cross section. The measured cross section σ_1 is put equal to the calculated cross section at v = 1180 m/sec. The monomer cross section at v = 1460, 810 and 760 m/sec follow from this choice and are then equal to the calculated ones within their errors. The dimer cross sections are obtained from the measured ratios σ_2/σ_1. The curves IIa and IIb are calculated for $C_{6,d} = 2.7\ C_{6,m}$ and $2.5\ C_{6,m}$ respectively, with $C_{6,m} = 2.80 \times 10^{-11}$ erg.Å^6; $\varepsilon R_m = 3.37 \times 10^{-14}$ erg.Å is taken equal for monomers and dimers.

temperature T_0 we find a limit pressure P_L below which the simple correspondence prevails. The values of P_L are collected in table IV.3. The limit pressure is of technical interest to those who want to design experiments. Therefore, we tried to condense our experience into a simple prescription using the intermolecular potential depth ε and the minimum position R_m as scaling parameters.

All our measurements on the noble gases Ar and Ne, and H_2 and N_2, performed with a $d_0 = 26\ \mu$ nozzle diameter, lead to P_L-values given by the following equation (within a factor 1.3)

$$P_L = 0.6 \times \varepsilon R m^{-3} . \{kT/\varepsilon\}^{(2-3\alpha)/(2-2\alpha)} . (R_m/d)^{.55} \qquad \text{(IV.2)}$$

Eq. IV.2 is not in contradiction with the general formulas given in ref. 8; actually, the temperature dependence correponds with the lower limit of Hagena and Obert. The temperature dependence for Ar and N_2 agrees, too, with the temperature dependence observed by Golomb et al. (ref. 9) for the pressure corresponding to the maximum of the dimer ion signal. At this pressure large clusters are abundantly present in the beam. Its value is about three times higher than the value of P_L, as can be seen from fig. III.1, or calculated from the experimental result and the scaling laws of ref. 9.

Eq. IV.2 is tested for $d = d_0 = 26\ \mu$, only. The last factor is added in view of the evidence (ref. 9) that beam condensation is determined by the product $P_0.d^{.55}$, at fixed source temperature. The scaling of the nozzle diameter d with R_m is in accordance with the principle of corresponding jets (ref. 8).

table IV.3

T_0	33	65	100	
Ne	100	600	1100	
H_2	90	600	1700	
T_0	123	173	223	294
Ar	300	600	1000	1800
T_0	133	173	223	294
N_2	800	1100	3000	–

Table IV.3. Values of P_L in torr at various T_0 for Ne, H_2, Ar, and N_2.

The dimer signal of NO forms an exception; here no contribution from fragmentation of larger clusters to the dimer ion signal is indicated by our measurements. At the maximum source pressure used many heavier clusters are present in the beam and the dimer ion signal levels off already.

IV.5. MAGNETIC DEFLECTION

We have looked for information concerning the magnetic properties of dimers of H_2, NO and O_2 in the beam by measuring their deflection in an inhomogeneous magnetic field.

For a well collimated H_2-beam at 26 K source temperature (v_1 = 750 m/sec) the ortho-monomers in the $m_I = \pm 1$ state can be bent off the beam axis. We have varied the position of a slit (.1 mm width) in front of the Rabi magnet. For a broad H_2-beam the three m_I-states are clearly resolved; at three different slit positions distinct maxima of the signal are observed (see also ref. 10).

Without a magnetic field the dimer beam is sharply peaked, corresponding to good collimation of the beam. With magnetic field on, a broad distribution is measured by varying the slit position. The f.w.h.m. of the distribution is equal to the separation of the two $m_I = \pm 1$ states for the monomer. This indicates that the H_2-dimers in the beam have magnetic moments comparable to those of the

H_2-monomers. Consequently, the H_2-dimers can be investigated by magnetic resonance spectroscopy, a method described in detail by Ramsey (ref. 11). The total signal of pure dimers amounts to 1% of the monomer signal at maximum.

In the liquid phase, dimers of NO are known to be diamagnetic; also solid NO is found to consist of diamagnetic NO-dimers. On the other hand, the paramagnetism of O_2 is preserved in the liquid phase. However, from analysis of magnetic susceptibility it has been suggested that in O_2 at low temperatures some molecules form nonmagnetic dimers (ref. 13). Knobler (ref. 14) has sought evidence for these nonmagnetic dimers in the liquid.

We have investigated whether gaseous dimers of NO and O_2 posses magnetic moments. The decrease of the dimer intensity due to the inhomogeneous magnetic field is compared with that of the monomer intensity.

For NO-monomers a slow monotonuous decrease is observed to about 40% of the full beam at the highest field gradient obtained in our experimental set up, about 20 kGauss.cm^{-1}. At low magnetic field no sudden decrease has been found due to the deflection of the $\Pi_{3/2}$-state. This agrees with the experimental result (ref. 15) that in a nozzle expansion the electronic temperature (calculated from the relative population of the $\Pi_{1/2}$ and the $\Pi_{3/2}$ states) decreases similarly to the translational temperature. In the highly expanded jet of our experiment the $\Pi_{3/2}$ -state may be completely depopulated.

For NO dimers no decrease because of the magnetic deflection is detected. The absence of a magnetic moment can be explained in two ways. If paramagnetic $\Pi_{3/2}$ molecules are present in the beam, it is not likely that they will form stable dimers with other molecules. The energy of the electronic excitation exceeds the binding energy of the dimer. Because many degrees of freedom are coupled in a dimer, this energy can be transfered to rotation and vibration, causing dissociation. We are left with the diamagnetic dimers of two $\Pi_{1/2}$ molecules only. On the other hand, assuming that a dimer containing one or two $\Pi_{3/2}$ molecules has a lifetime long enough to reach the detector, its magnetic moment will be averaged to zero by the end over end rotation, in first order. For the end over end rotation large quantum numbers are allowed, see sect. VI.3.

The O_2-monomer signal drops to about 30% of its maximum value at low fields already, due to the deflection of the $^3\Sigma(m_s = \pm 1)$ states. At higher fields the signal approaches zero because the $^3\Sigma(m_s = 0)$ state is also deflected now, due to its small magnetic moment originating from the rotation of the molecule coupled to the electronic spin. We observe that O_2 dimers can be deflected, too; the maximum obtainable decrease of signal is about 70%. Therefore, O_2 dimers are paramagnetic. We consider the dispute about the appearence of diamagnetic O_2 dimers as settled (ref. 14). There are none.

Paramagnetic O_2-dimers will be interesting objects for a magnetic beam resonance study, although intensity problems may be severe. Admixture of He may improve the situation (see sect. VII.4).

REFERENCES CHAPTER IV

1. A. v. Deursen, A. v. Lumig and J. Reuss, Int. J. Mass Spectrom. Ion Phys., *18* (1975) 129, ch. III of this thesis.
2. A. v. Deursen and J. Reuss, Int J. Mass Spectrom. Ion Phys., *11* (1973) 483, ch. II of this thesis.
3. R. Helbing, W. Gaide and H. Pauly, Z. Physik, *208* (1968) 215.
4. F. v. Busch, Z. Physik, *193* (1966) 412.
   F. v. Busch, H. J. Strunck and Ch. Schlier, Z. Physik, *199* (1967) 518.
5. R. B. Bernstein, Comments At. Mol. Phys., *4* (1973) 43.
6. L. D. Landau and E. M. Lifshitz, "Quantum Mechanics", Pergamon Press, London (1959).
7. Calculations performed by L. Zandee, using a computer program of H. Moerkerken.
8. O. F. Hagena and W. Obert, J. Chem. Phys., *56* (1972) 1793.
9. D. Colomb, R. E. Good, A. B. Bailey, M. R. Busby and R. Dawbarn, J. Chem. Phys., *57* (1972) 3844.
10. L. Nelissen, J. Reuss and A. Dynamus, Physica, *42* (1969) 619
11. N. F. Ramsey, "Molecular Beams", Oxford University Press, New York (1956).
12. H. Bizette and B. Tsai, Compt. Rend., *204* (1937) 1638.
13. G. N. Lewis, J Am. Chem. Soc., *46* (1924) 2027.
14. C. M. Knobler, Thesis, Leiden (1961).
15. S. Stolte, private communication.